Using Dark Fiber and Distributed Acoustic Sensing for Near-Surface Characterization and Broadband Seismic Event Detection

Jonathan B. Ajo-Franklin[1,*,+], Shan Dou[1,+], Nathaniel J. Lindsey[1,2,+], Inder Monga[3], Chris Tracy[3], Michelle Robertson[1], Craig Ulrich[1], Barry Freifeld[1], Tom Daley[1], and X.S. Li[4]

[1]Lawrence Berkeley National Laboratory, Energy Geoscience Division
[2]University of California, Berkeley, Earth and Planetary Sciences Department
[3]Lawrence Berkeley National Laboratory, Energy Sciences Network
[4]Lawrence Berkeley National Laboratory, Computational Research Division
[*]jbajo-franklin@lbl.gov
[+]these authors contributed equally to this work

ABSTRACT

We present the first case study demonstrating the use of regional unlit fiber-optic telecommunication infrastructure (dark fiber) and distributed acoustic sensing for broadband seismic monitoring of both near-surface soil properties and earthquake seismology. We recorded 7 months of passive seismic data on a 27 km section of dark fiber stretching from West Sacramento, CA to Woodland, CA, densely sampled at 2 m spacing. This dataset was processed to extract surface wave velocity information using ambient noise interferometry techniques; the resulting V_s profiles were used to map both shallow structural profiles and groundwater depth, thus demonstrating that basin-scale variations in hydrological state can be resolved using this technique. The same array was utilized for detection of regional and teleseismic earthquakes and evaluated for long period response using records from the M8.1 Chiapas, Mexico 2017, Sep 8th event. The combination of these two sets of observations conclusively demonstrates that regionally extensive fiber-optic networks can effectively be utilized for a host of geoscience observation tasks at a combination of scale and resolution previously inaccessible.

Introduction

Hydrogeologic and seismological data collection are two domains for which the absence of high spatio-temporal resolution data is particularly acute, with significant impacts on our ability to characterize near-surface soil properties, groundwater systems, and seismic events. Even relatively basic subsurface hydrological parameters such as water table depths in surficial aquifers suffer from severe undersampling in both space and time. While heavily monitored basins often have a multitude of wells providing subsurface access, they are neither uniformly distributed nor frequently monitored resulting in heterogeneous datasets requiring manual quality control, curation, and analysis. The few basin-wide hydrogeological data sources, typically based on satellite remote sensing technologies, provide only surficial property estimates like soil moisture[1,2], integrated strain response (e.g. InSAR[3]), or low-resolution volumetric datasets (e.g. GRACE,[4,5]) which require assimilation with point measurements to provide finely resolved operational parameters (e.g.[6]). Remote sensing measurements often also suffer from temporal undersampling due to satellite pass frequency. More recently, seismic ambient noise interferometry[7] has been leveraged to provide broader information on ground water storage; unfortunately limited permanent seismic networks present a challenge for these approaches.

Likewise, seismological data collected using existing permanent networks often have spatial regions which suffer from significant spatial undersampling, particularly in areas distant from major plate boundaries, resulting in challenges when attempting to detect and locate small natural and induced events. The case of small magnitude induced events is particularly problematic since the basins where oil and gas production, wastewater injection, and carbon dioxide sequestration occur are often distant from historically seismogenic faults and the associated permanent seismic networks. Network sparsity increases the minimum event size for detection, results in statistical biases in the catalog, and greatly increases depth uncertainty for local events. Recent studies focusing on seismic catalog completeness in California have determined that even M2 events cannot be detected in the majority of the Sacramento and San Joaquin Basins using the existing network stations[8].

These spatio-temporal undersampling problems, for both hydrological and seismological measurements, can be remedied by re-purposing ubiquitous sensing platforms already deployed at scale. A recent example of such an approach is the utilization of smartphone accelerometers to measure strong ground motion as part of earthquake early warning applications as shown

by[9] and[10]; other examples include using social media proxies as sensors (e.g.[11]) or MEMS accelerometers in pervasive stationary devices such as personal computers ([12]). Broader efforts to leverage networking and sensor technologies related to the Internet-of-Things (IoT) for seismology are developing but still in their infancy (e.g.[13]).

An alternative approach is to exploit components of the built environment to serve as distributed sensor networks. In this case we explore the use of unlit subsurface fiber-optic cables, commonly referred to as "dark fiber", and distributed acoustic sensing (DAS) to provide such a spatially extensive sensing platform. The vast majority of fiber-optic cables in the earth's near-surface were installed exclusively for the purpose of telecommunications. Due to high cost of fiber-optic installation, typical commercial practice is to deploy significantly more capacity, as measured by fiber count, than required; this practice, combined with advances in bandwidth available per fiber, have yielded a surplus of available fibers that remain unused. The US footprint of such unused fiber networks is massive with tens of thousands of linear kilometers of long distance fiber-optic cables available for lease or purchase in the current environment. One notable aspect of such dark fiber network components is that they tend to utilize existing "right-of-way" corridors along roads and rail connections ([14]), environments rich in ambient noise. Given the ubiquitous nature of installed telecom fibers, few studies have explored use of this resource for sensing applications. A single experiment explored the use of Brillouin Optical Time Domain Analysis (BOTDA) to monitor temperature over previously installed telecom fiber ([15]); however, these studies were conducted primarily to provide network integrity information rather than for environmental sensing.

Distributed Acoustic Sensing (DAS) is a recently developed technique which utilizes coherent optical time-domain reflectometry to accurately measure the phase and amplitude of vibrations along an optical fiber. The technique exploits changes in Rayleigh scattering induced by extensional strain; these measurements have now been quantitatively compared to point seismic recordings at both intermediate ([16]) and low frequencies ([17]) and utilized for a host of tasks including vertical seismic profiling ([18,19]), near-surface soil property estimation ([20–22]), and earthquake observations ([23,24]). DAS has created a recent paradigm shift in applied geophysics by enabling seismic measurements at a combination of high frequency (kHz range), distance (tens of km), and spatial sampling (as small as 1 m), a combination previously unavailable with conventional sensors at moderate costs. While prior studies have convincingly demonstrated the value of dense networks for seismic imaging and a range of other purposes (e.g.,[25]), the high logistical cost massive nodal deployments over long time periods has precluded their use in many contexts.

In this study, we demonstrate the utilization of DAS coupled to dark fiber for measurement of seismic wavefields at the sub-basin scale with an extremely fine spatial sampling (2 m) over long time periods; the resulting ultra-dense dataset is utilized for both hydrogeological/near-surface characterization, using ambient noise interferometry, and the detection of seismic events, both local and global. This combination is perhaps a new frontier which leverages investment in built infrastructure to greatly extend the reach and sampling of existing permanent monitoring networks.

Seismic Monitoring with Dark Fiber Networks

Our study utilized dark fiber components of ESnet's Dark Fiber Testbed. ESnet, a US Department of Energy (DOE) user facility, provides high-performance unclassified network infrastructure to connect DOE research sites including high performance computing (HPC) facilities and data-intensive instrumentation e.g. x-ray, neutron, and nanoscience facilities. The Dark Fiber Testbed is a 20,920 km (13,000 mile) network of short and long haul telecommunication fiber designed for testing novel network communication equipment and protocols. The network consists of single mode telecommunication fibers of varying age and installation technologies and hence is an excellent proxy for existing commercial network components. This study is the first experiment that utilizes this massive network for sensing purposes. Figure 1, panel A, depicts the long haul regional sections of the Dark Fiber Testbed in California, as well as the segment exploited for our test (panel B) which runs from West Sacramento CA to Woodland CA.

Field Deployment

The site of our study was a transect located in the Sacramento River flood plain, north and west of Sacramento, CA. The geology of the site consists largely of Quaternary sediments including a sequence of silts and clays underlain by fine sands. Partially lithified sediments from the Tehama formation have been mapped from approximately 50m to greater depths (Olmsted and Davis, 1961). The segment of dark fiber we utilized for this study, shown in Figure 1 panel B, runs from West Sacramento CA to the small town of Woodland CA. As can be seen from the fiber network map, the recording profile extends from an urban environment into a section of farmland near the Sacramento River, crossing Interstate 5 before bending westward towards Woodland. The agricultural areas sampled by this profile are partially irrigated through a variety of methods and groundwater is actively extracted from both the shallow surficial aquifer as well as deeper sources.

The seismic dataset presented in this study was recorded between July 28th, 2017 and Jan. 18th, 2018. The DAS interrogation unit (IU; Silixa iDAS, Elstree, UK) was installed in a telecommunication Point-of-Presence (PoP) facility in West

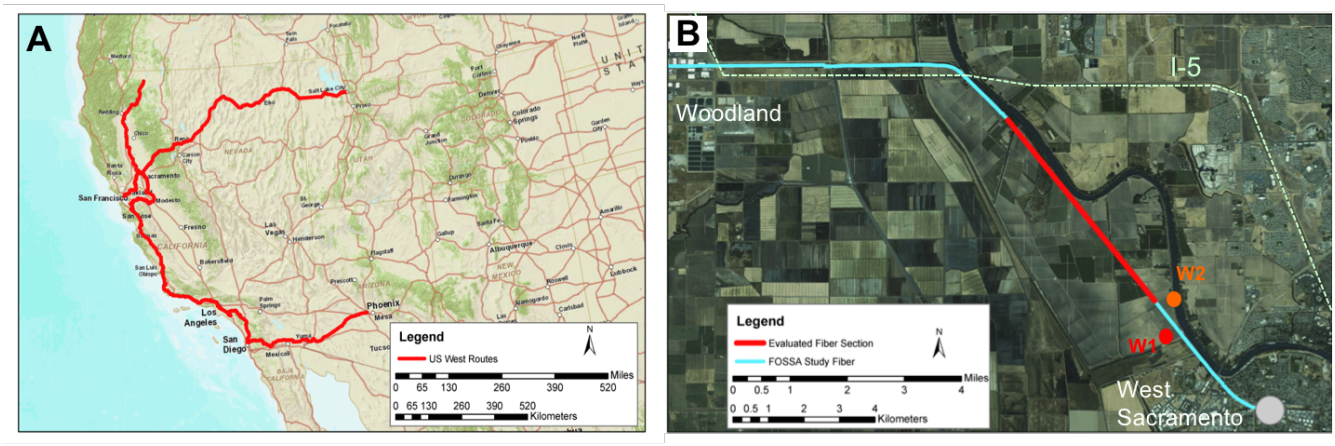

Figure 1. Map of a section of the ESNet Dark Fiber Testbed (https://www.es.net/network-r-and-d/experimental-network-testbeds/100g-sdn-testbed/terms-and-conditions/). (A) The regional network within CA and western NV. (B) The subsection of the network used in this study. The red segment in (B) is the area of focus for ambient noise analysis; W1 and W2 are reference wells for water table and soil horizons, respectively

Sacramento. Hardware details on the installation are described in Methods Section 0.2. Ambient seismic noise was recorded using the DAS IU at 500 Hz sampling with a spatial sampling of 2 m and a 10 m gauge length. Data was streamed continuously to large capacity (8TB) external hard drives that were exchanged on a weekly basis.

While the surface geometry of the dark fiber network was known before deployment, the mapping to linear fiber location was established by sequential impact tests at surface locations surveyed with high accuracy differential GPS. This is necessary due to the common practice of including spools of slack cable during telecom installation, an approach that makes the mapping of surface geometry to linear fiber location more complicated. The resulting geometry likely has an uncertainty on the order of 5m due to the interpolation process along the transect.

After the network geometry was established, DAS signal strength, amplitude, and periodicity were examined to evaluate noise characteristics along the array. Dominant noise features include several regional highways, diffuse urban noise, and energy from local railroad activity. The highest quality data was obtained from a straight section of fiber starting beyond West Sacramento and extending to the noise field of Interstate 5, shown as the highlighted red profile in Figure 1, panel B.

High Resolution Kilometer-Scale Near-Surface Imaging Using Ambient Noise

Prior studies have demonstrated the potential of utilizing ambient noise interferometry and classical sensors to detect fluctuation in groundwater state (e.g.[7]). Ambient noise interferometry is an established class of algorithms that utilizes environmental vibrations from either near-surface or subsurface sources to retrieve coherent seismic information, referred to as empirical Green's functions. More recently,[20] demonstrated that such techniques could be utilized to transform infrastructure noise in the 2-30 Hz band (e.g. surface waves generated by cars, trucks, and trains), into accurate and stable 1-D estimates of shear wave velocity from 0-30 m depth using DAS. While[20] examines data acquired on a fit-for-purpose array, the processing strategy proposed can be easily adapted to dark fiber deployments.

The present study images near-surface shear wave structure using infrastructure noise generated by freight trains operating along a 6600 m subsection of the dark fiber array (Fig. 1B). Similar to our earlier work which exploited road noise, we use ambient noise interferometry to transform the raw noise records into virtual common-shot gathers; we then apply the multichannel analysis of surface waves (MASW) analysis to infer shear-wave velocity (V_s) profiles with a multimodal inversion strategy. Figure 2 is an illustration of this workflow (see Supplementary Fig. 9 for more details).

The results are a series of V_s profiles, each representing 1-D approximations of the subsurface underneath each of the 120-meter-long fiber subsections (Fig. 3). As is to be expected, the installation conditions of the dark fiber are not always ideal for V_s imaging, hence gaps are left in the pseudo 2-D section shown in Fig. 3b. However, with 57% of the 6600-meter-long fiber transect providing useful data, our lateral coverage of 3760 meters warrants its place as the longest MASW profile ever obtained using ambient noise alone. Comparisons to our limited ground truth database reveal that the interfaces of the V_s profiles match reasonably with the groundwater level and deeper lithological horizons, which confirms the validity of the inversion results. The lithological horizons consist of transitions from near-surface silty clay units to deeper sand and gravel units as inferred from drilling logs from a local water well W2, as shown in Fig. 3B.

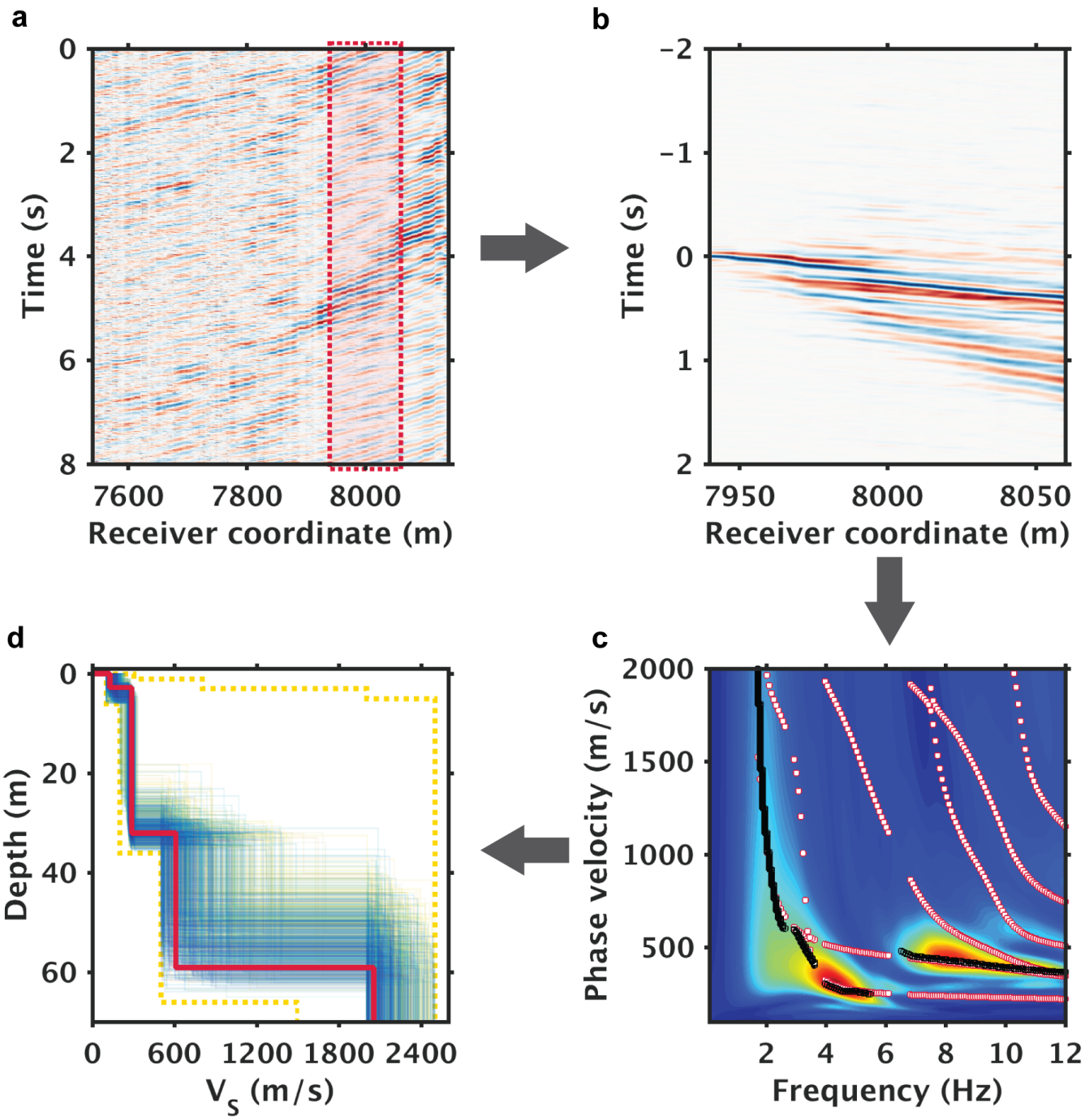

Figure 2. Illustration of data processing workflow for ambient noise interferometry. (a) Example of train noise shown via an 8-second slice. The red box in (a) highlights subsection of the array used for (b) noise correlation, (c) dispersion analysis, and (d) inversion of the shear-wave velocity profile. Black and white markers in (c) denote observed and model-predicted multimodal dispersion curves. In (d), the yellow dashed lines denote upper and lower bounds of the parameter space used in Monte Carlo sampling; the bold red line marks the topmost best-fitting profile and the yellow/blue lines denote the top 0.1% best-fitting profiles.

Moreover, because V_s30 (the travel-time average of V_s over the top 30 meters), a widely used indicator of seismic site conditions6, 7,) is readily obtainable from the V_s profiles, both the values and the lateral variations of V_s30 are useful data products that the dark fiber array can provide.

To evaluate the utility of the DAS ambient noise inversion results for hydrogeological monitoring, we compare the transition in V_s identified as the water table to direct point measurements in the one well with sufficient temporal sampling information located on our transect. The well (W1) is located at the southeastern end of the high S/N section of dark fiber near the intersection of County Road 126 and the Old River Road, shown as a red dot on figure 1b. Water level in this well varies by as much as 7.6 m (25 ft) over annual hydrologic cycles and is impacted by Sacramento River levels, agricultural irrigation and surficial aquifer pumping. As can be seen in Figure 3a (top), the depth of the first V_s increase (4 m below surface) correlates to the measured surficial water table depth (blue line in figure 3b). We should note that an increase in V_s at the water table is not predicted by classical rock physics models which assume that shear modulus is not sensitive to saturation; despite this, past field studies (e.g.[26]) have provided detailed observations of such sensitivity, presumably due to the impact of moisture on soil cohesion.

Time-Lapse Monitoring of Groundwater Level

As mentioned previously, the Sacramento Basin is a dynamic hydrologic environment with multiple productive aquifers, active groundwater production, irrigation, and river interactions. Besides static profiles quantifying V_s, the dark fiber array also allows for time-lapse monitoring of the subsurface, enabling measurement of hydrologic transients in the near-surface. Traditionally, because sensors are rarely dense enough for imaging, time-lapse monitoring results are typically presented as an apparent-velocity perturbation along the path connecting two sensors8, 9 without identifying where on this path the changes are occurring. This level of detail is insufficient for proactive management of groundwater resources, given that both vertical and lateral changes of the groundwater level could affect the overall sustainability of the aquifer. With the dark fiber array enabling time-lapse imaging of the near surface, changes in groundwater levels could be resolved with spatial-temporal resolutions pertinent to groundwater management.

Figure 4 demonstrates the repeatability of time-lapse imaging chiefly by comparing the groundwater levels retrieved from a monitoring well against what were obtained from the closest dark-fiber section. Note that no major rainfall events had occurred during the three-month monitoring period processed for this study, and as a result, the maximum changes in the measured water table did not exceed 0.9 m. The high repeatability of interferometric gathers, both in the offset-time domain (Fig. 4a) and frequency-velocity domain (Fig. 4b) suggests that such levels of variation will not be resolvable using this approach. An inspection in the model space (Fig. 4c) confirms the inversion's insensitivity to these sub-meter changes. However, such repeatability provides assurance for reliably resolving larger changes in groundwater levels, because the well data, when examined over a year-long period, exhibit groundwater level changes up to 8 m. Such marked changes should be resolvable with the dark fiber array with a more extended monitoring period.

Earthquake Seismology with a Dark Fiber DAS Array

Seismic network detection thresholds are highly heterogeneous, even across regions known for dense seismic monitoring like the western United States and Japan ([27,28]), in part because broadband seismic stations are sited in hard-rock locations where background noise is low ([29,30]). Areas of less-competent geology, like sedimentary basins, therefore correlate with poor catalog completeness; the magnitude of completeness is Mc 2 – 3 in the Sacramento and Southern San Joaquin Basins compared to Mc 0.5 – 2.4 in the San Francisco Bay Area or Mc 0.5 – 1.8 in Southern California ([8,31,32]). Thus, despite the greater Sacramento area hosting significant gas production, underground gas storage and high-volume waste water disposal, all of which can impact seismicity, the Sacramento Dark Fiber DAS array is located 30 km away from the nearest networked short-period seismometer (NDH) and 62 km away from the nearest broadband seismometer (AFD).

A relevant question when examining seismic events on telecommunications networks in contrast to fit-for-purpose installations is the impact of installation conditions. As recently demonstrated[23], fiber installation in a standard plastic conduit does not preclude sufficient sensor coupling required for the detection of earthquakes, but the case of recording DAS data with repurposed telecommunications fiber is yet untested at regional scales. To explore this question with the Sacramento Dark Fiber DAS experiment we extract raw strain-rate waveforms for major global and regional earthquakes that occurred during the continuous recording interval (Fig. 5). We again use the linear quiet portion of the array shown in Fig. 1B and process the data by averaging 100 seismic traces (200 m section) and applying a bandpass filter to isolate the appropriate earthquake signals. We observed broadband DAS sensitivity to ground motion from earthquakes of varying magnitudes (M4.4 – M8.1) and distances (100 – 7757 km). For example, in the case of the M7.5 Honduras event there is clear evidence of short period body waves and longer period surface waves over the two hour window following the origin.

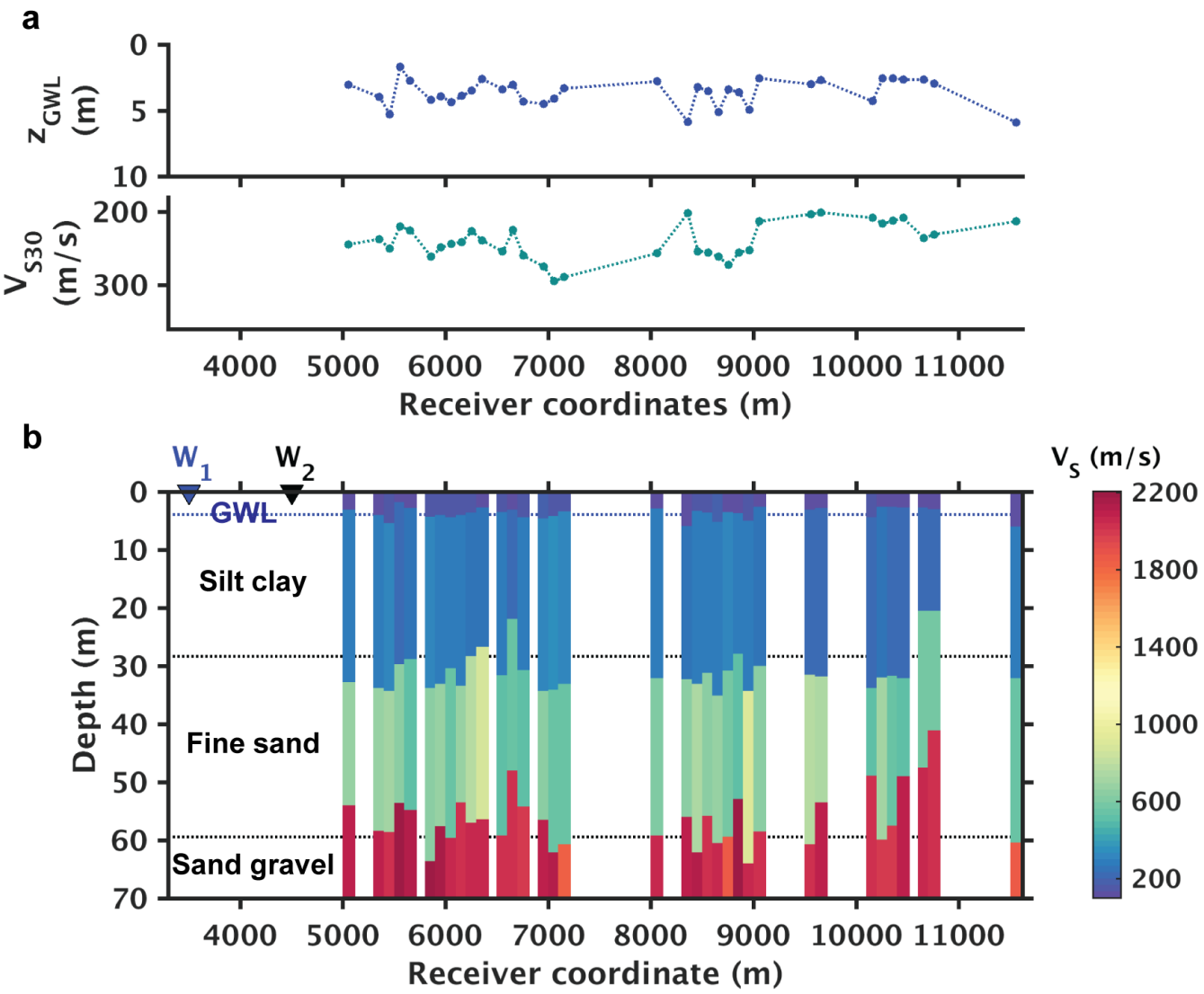

Figure 3. Shear-wave velocity (V_s) inversion results and ground truth comparison. (a) Depths of groundwater levels (GWL) (upper) and V_s30 estimates (lower) extracted from the inversion results. (b) Pseudocolor display of V_s profiles and comparisons against well data. In (b), W1 and W2 mark surface locations of the two reference wells shown in Fig.1; The blue dashed line denotes the depth of the ground water level provided by water well W1; the black dashed lines correspond to lithological horizons obtained from geotechnical well W2.

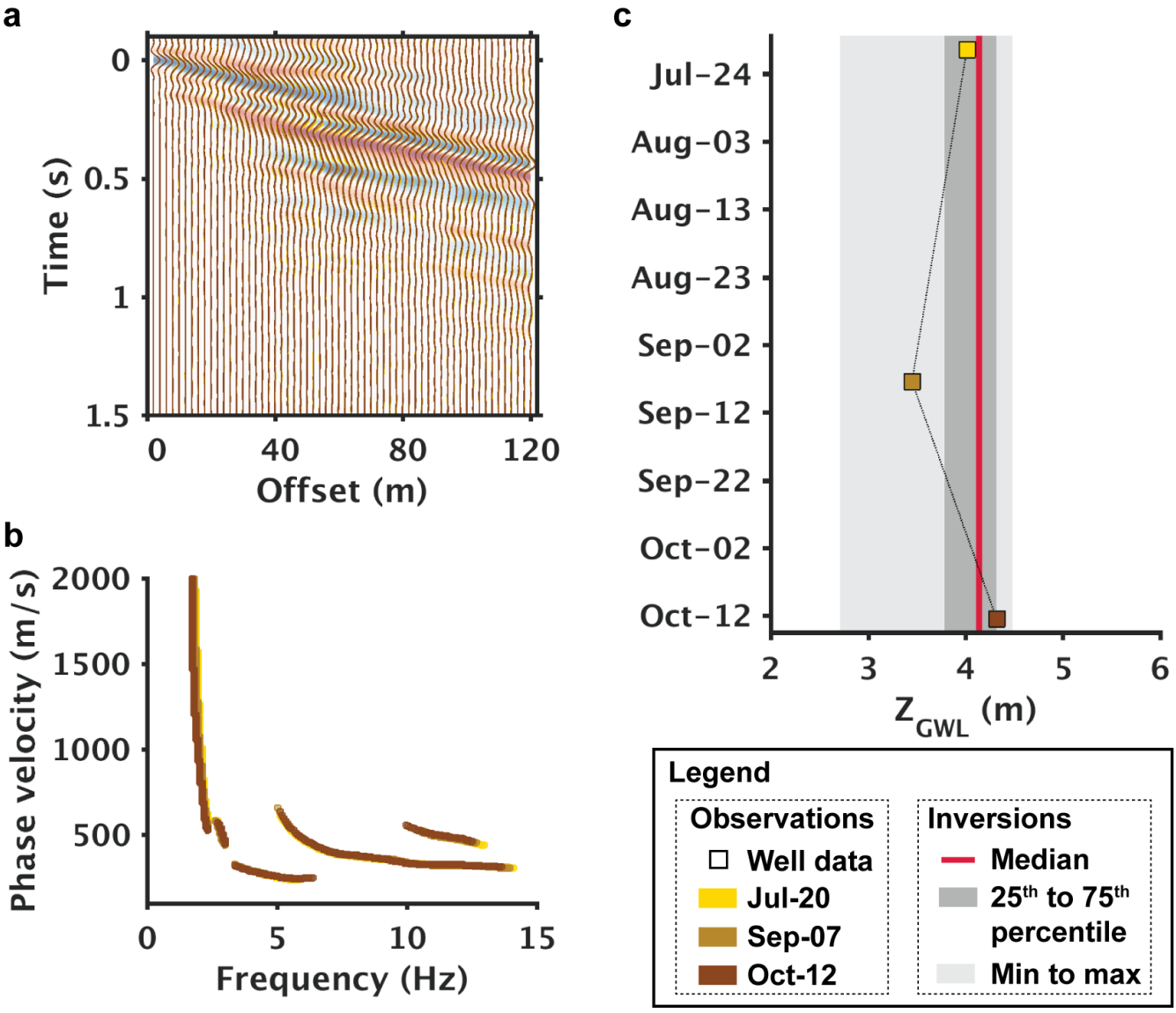

Figure 4. Time-lapse repeatability demonstration of ambient noise analysis in (a) space-time domain, (b) frequency-velocity domain, and (c) in terms of groundwater levels obtained from the model domain. Color transitions from the yellow to brown denote chronological orders of the monitoring period. In (c), the median, min-max range, and percentiles are calculated based upon all the topmost best-fitting models associated with the monitoring period.

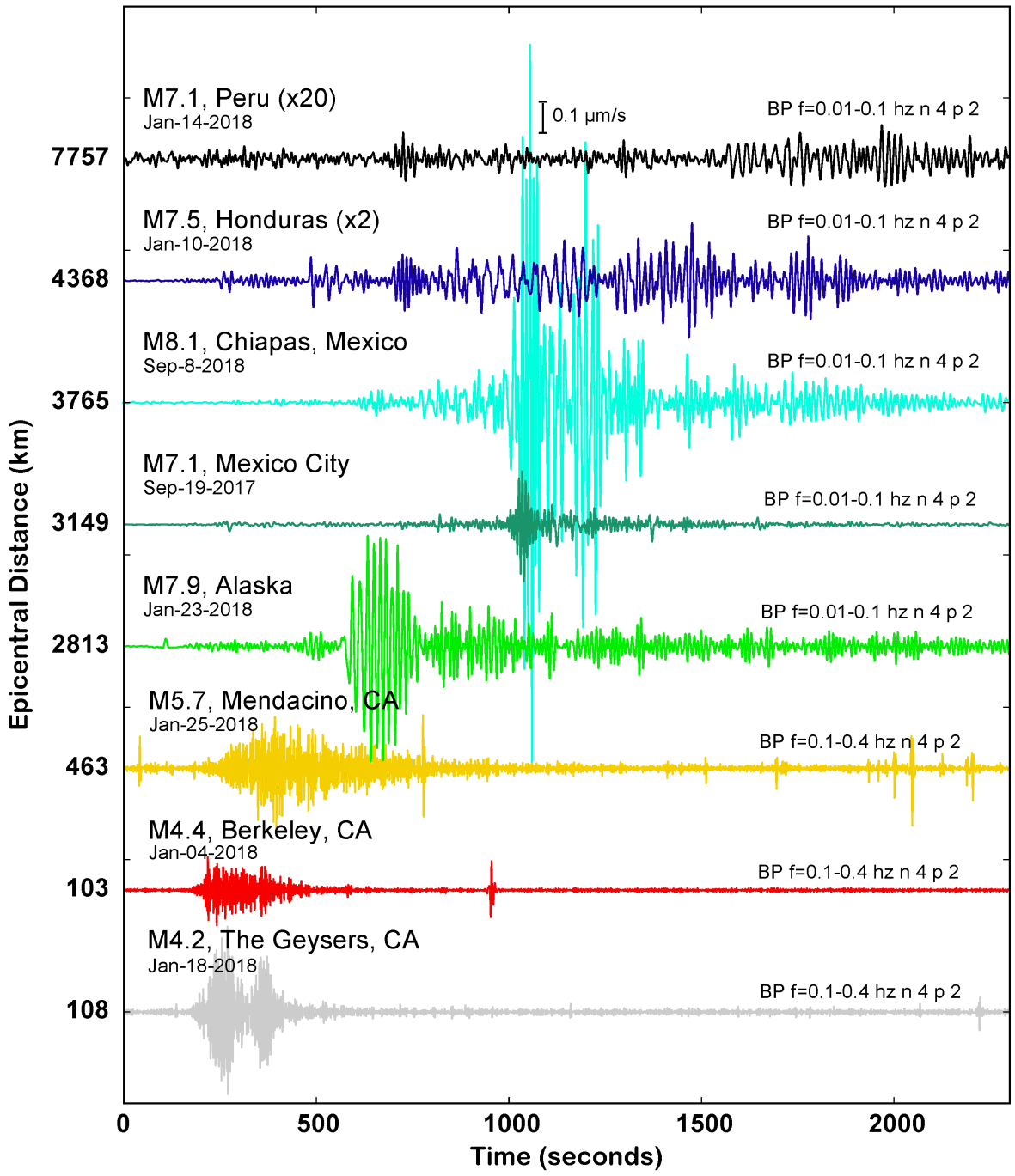

Figure 5. Example earthquakes recorded by the Sacramento Dark Fiber DAS array. The recorded data are shown as strain-rate (nm/s) averaged over 100m (50 seismic traces) and bandpass filtered in the 0.1-0.4 Hz range for regional events, and 0.01-0.1 Hz for teleseisms. Events are sorted by increasing epicentral distance from Sacramento. Earthquake amplitudes for the Peru and Honduras events are scaled by the factors in parentheses.

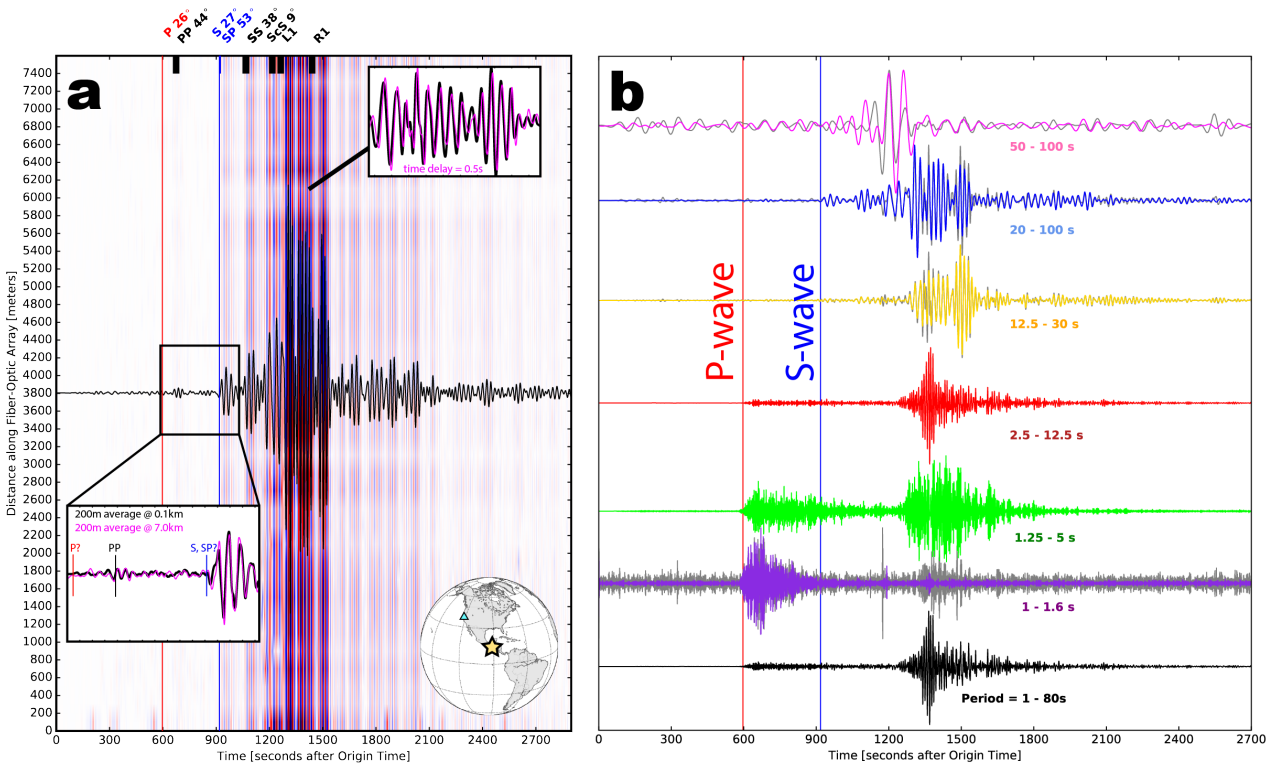

Figure 6. Teleseismic DAS recording of the M8.1 Chiapas, Mexico 2017-Sep-08 earthquake. (a) Seismic data for [black trace] one location and [red and blue] all locations from 0.0-7.6 km at a 2 m spacing (4001 traces total); top right inset shows surface waves arriving at the [black] south and [pink] north end locations of the array (backazimuth 120o), bottom left inset shows body waves arriving coincidently at both locations. A two-corner, zerophase, f= 0.01 – 0.5 Hz bandpass filter was applied. (b) Stacking 400m or 200 consecutive DAS channels, color-coded by the bandpass filter applied to emphasize the broadband observation (1-100 seconds). Gray background traces show the single trace recording for cases that make a significant difference. Each of the traces is normalized to peak amplitude.

While long period sensitivity is a major limitation of many inertial seismic sensors (e.g., accelerometers, short-period geophones, smartphone sensors), the long period response of DAS is currently a topic of active research with only limited available data[17]; teleseismic earth motion (strains near 1×10^{-8}), for example, may be dominated by thermal expansion of the fiber-optic cable (strains on the order of 1×10^{-6}) depending on the frequency studied as well as the depth, composition, and condition of the fiber-optic cable and conduit.[17,33] used a shallow hydrogeologic pump test in a well with a fiber-optic cable to show that DAS has sensitivity to 9.4×10^{-3} Hz (period = 1080 seconds) oscillations in strain induced by the variable confining pressure, presumably due to Poisson effects. This subject is complicated by the known directionality of DAS cables ([34,35]), which for the horizontal geometry of telecommunications dark fiber cables is theoretically insensitive to vertically-incident compressional motion (P-waves).

To explore the long period sensitivity of the Dark Fiber DAS array to teleseismic events, we extract raw strain-rate seismograms from the largest earthquake recorded during the experiment, the M8.1 2017-Sep-08 Mexico earthquake (Fig. 6). We observe broadband dispersive surface waves with strong energy at periods from 50 – 100 seconds. P-wave signal amplitude is lower than S-wave amplitude, perhaps because the sensor has minimal sensitivity to compressional particle motions for waves with incidence angles approaching 0^o with respect to vertical (i.e., perpendicular to the fiber, so-called "broadside arrivals"). Nonetheless, the arrival times of major seismic phases are detected because of free surface scattering. Incidence angles of seismic phases are given in Figure 6a [top]. Differences in incidence angle also likely affect recorded amplitude, and appear to result in more coherent surface wave arrivals across the array (incidence angle=0^o) and as much as a 0.5 second delay time across the record section.

Telecommunications cables are commonly routed along railways, roads, and through high noise urban areas. We find that

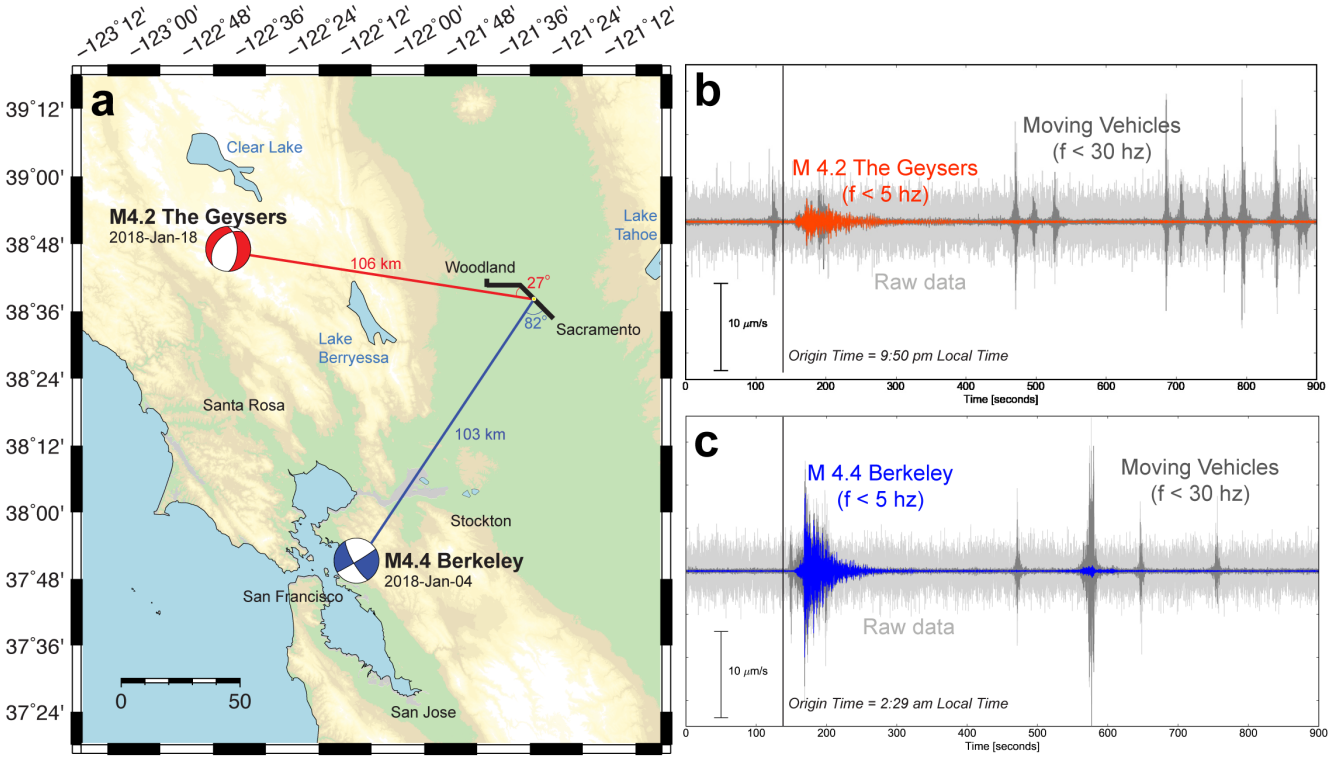

Figure 7. (a) Locations and focal mechanisms of the M4.2 2018-Jan-18 Geysers (red) and M4.4 2018-Jan-04 Berkeley (blue) earthquakes, which occurred approximately 100 km from the Sacramento Dark Fiber DAS array (black line). (b,c) Raw and lowpass filtered DAS strain-rate waveforms for these events averaged over 100 m (50 channels) at the yellow circle position shown in (a) (channel 4975 +/- 50 channels). Note the similarity between seismic and non-seismic signal amplitudes and the differences in frequency content.

major regional earthquakes (M 4) generate ground motions on the Sacramento array that have equal or lesser amplitude than local moving vehicles, however the non-seismic signals typically are dominant in a higher frequency band (5 – 30 Hz). Figure 7 shows how the seismic signals from two different regional earthquakes (M4.22 Geysers 2018-Jan-18 and M4.38 Berkeley 2018-Jan-04) are easily discriminated from the local noise field based on spectral content. Higher frequencies of interest for local microearthquake analysis (f ¡ 50 Hz) will not always separate in this way.

The two earthquake records shown in Fig. 7 appear very different despite having been generated in similar sized ruptures and traveled similar distances to Sacramento. This may be due to source rupture depth differences (z=2.4 km for The Geysers, z=12 km for Berkeley), but could also be the result of strong DAS axial sensitivity to energy in the direction of the fiber axis, resulting in larger recorded amplitudes for shear waves from Berkeley than from The Geysers, but larger recorded amplitude for Rayleigh waves from The Geysers because of the more favorably oriented polarization.

We hypothesize that the method of installation (direct-burial, single conduit, conduit inside a larger conduit, conduit attached to infrastructure) has a significant effect on DAS recorded ground motion (see Fig. 8). The fiber-optic cable itself (gel-filled, aramid wrapped vs. loose-tube, polyethelene-jacketed vs. steel-armored, polyethelene vs. steel exterior) has each been shown to have only a small effect on recording quality at high frequencies ([20]).

Installation information for the Sacramento Dark Fiber DAS array provides clues to the dataset's heterogeneous fiber-soil coupling profile. Cable installation occurred in 1999-2000. Most of the fiber was pulled through one of 12 high-density polyethelene (HDPE) conduits (ID = 3.5 – 4cm, wall thickness = 0.5 cm) that were buried together in a trench at 1 – 1.5 m and backfilled with soil before installing the fiber cable inside. Each fiber cable contains 84 gel-filled, loose-tube Corning LEAF fibers that are polythelene jacketed and steel-armored. The DAS data were recorded using one 9/125 μm single-mode fiber from one of these cables. In a few locations, trenching was not possible so directional boring was used to install a large casing conduit (ID = 20-25 cm, wall thickness = 0.4 cm), inside of which the 12 smaller conduits were pulled. Depth of boring varied between one meter and a few meters when navigating around various culverts, sections of road and railway, or another obstacles. In some instances the casing was not required, or a steel casing may have been used. A third mode of installation used for

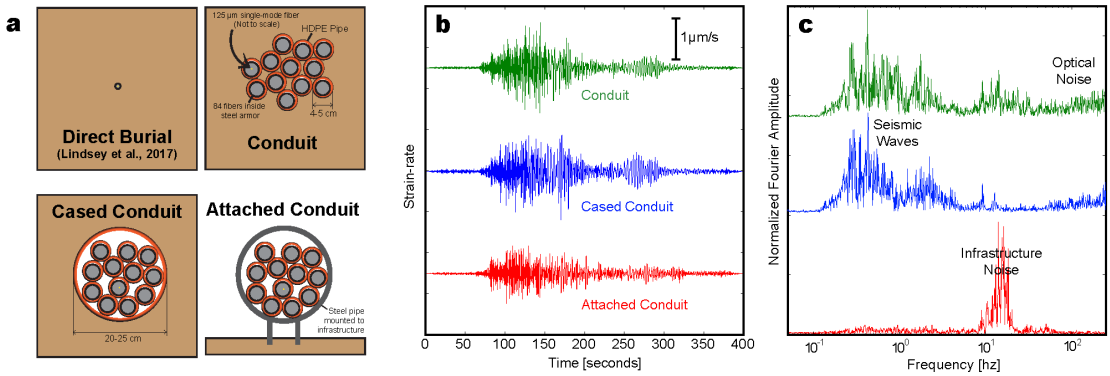

Figure 8. (a) Illustration of different installation geometries. (b) Earthquake (M4.2 Geysers 2018-Jan-18) trace comparison for each installation mode at Sacramento – trenched conduit (green), cased conduit (blue), attached conduit (red); strain-rate data are stacked over 100m and filtered (BP 0.5 – 2 Hz n 4 p 2). (c) Normalized Fourier amplitude spectra for the waveforms shown in b.

approximately 300 m of the dark fiber array involved attaching a 20 – 25cm diameter steel casing directly to the elevated rail line where it crosses a steep ravine. Inside this attached conduit the 12 HDPE conduits were installed as the boring method described above.

Fig. 8 shows DAS strain-rate earthquake waveforms (BP 0.5 – 2 Hz n 4 p 2) and normalized Fourier amplitude spectra for the M4.2 Geysers 2018-Jan-18 event stacked over 100m of each of the three install modes. Any phase shifts between traces are due to these install locations being separated by as much as 7 km along the array. The conduit and cased conduit data show very similar seismic wave response to the ground motion centered in the f=0.1 – 10 Hz range. Seismic signal amplitudes are observed to be on order with the optical noise at f $>$ 100 Hz. Data from attached section are noisier in a narrow frequency band centered on 12 Hz +/- 3 Hz, perhaps caused by interaction of the incident seismic energy with the infrastructure and/or tube waves traveling in the attached conduit at air velocity. The trenched conduit shows a broader spectral response to near-surface scattering into surface waves, while the cased conduit is relatively insensitive to it.

Discussion

As demonstrated in the prior sections, DAS-based seismic measurements acquired using dark fiber can provide a wealth of information relevant to near-surface seismic property estimation, hydrologic state, and natural seismicity. Measurements using dark fiber also have advantages in a host of situations ranging from marine to urban scenarios where classical seismic networks are challenging to execute.

An obvious strength of dark fiber DAS deployments, demonstrated in this study, is the potential to record data across long (10s of km) transects at high spatial resolution without any required sensor installation or power source. Chains of such deployments could be utilized to provide true basin scale sensing; the Sacramento Basin's central width (120 km) could be spanned using only 4 independent interrogation units and existing dark fiber resources, providing an unprecedented sensing resource. While basin scale hydrogeophysical monitoring studies using point sensors and ambient noise have been recently conducted (e.g.[7]), the spatial resolution of such investigation is typically on the order of km due to sparse sensor distribution. Recent advances in large N processing approaches (e.g.[36]) also offer strategies for leveraging dense arrays for detecting small seismic events.

A second advantage of utilizing dark fiber for seismic measurements is dense non-invasive coverage in urban areas where diverse deployment and permitting environments challenge classical acquisition strategies. The present study provides coverage

spanning urban (Sacramento), suburban, and rural zones without the typical landowner permission effort, permitting, and survey work required for deployment in occupied areas.

While not demonstrated in this study, dark fiber can also be utilized for observations in the transition zone and offshore domains, areas where almost no measurements exist at present due to the high cost of tethered marine observatories including seismometers. Offshore DAS measurements would be particularly useful for improving the hypocenter accuracy for small events occurring on marine faults and earthquake early warning in subduction zones. Limitations of using DAS and dark fiber for offshore observations include (a) distance constraints for DAS measurements on single mode fiber for existing optical chains, currently in the range of 30-40 km, (b) the considerably higher cost for dedicated use of fibers in transoceanic cables, (c) the lower density of offshore cable routes which reduces coverage. Having said this, offshore dark fiber recording provides a clear future opportunity to extend the domain of seismological measurements into previously uninstrumented regions.

Despite these opportunities, challenges exist to fully exploit these conceptually novel sensing networks. Extremely large data volumes are among the most pressing, although solvable, problems; at maximum acquisition rates, a single interrogator can generate upwards of 20 TB/day. Combining these large N deployments with the long time periods required for ambient noise processing and monitoring yields raw data volumes that exceed the capacity of the computational infrastructure available to most researchers. The array in this study, which included 12000 channels sampled at 500 Hz, generated 128 TB of raw data in the first 3 months of operation and approximately 0.3 PB of raw data when the system was demobilized. Volumes of this size require careful consideration of data transport requirements, storage, archiving, and automated processing to be successfully utilized. Fortunately, on-going efforts to solve I/O and computational barriers in ambient noise studies ([37,38]) provide a path to potentially handle the much larger datasets generated by dark fiber studies.

Methods

0.1 DAS system installation

The Silixa iDAS unit was installed on a vibration isolated table located in the West Sacramento PoP. Vibration isolation consisted of a 18 x 24" Nexus Breadboard (Thorlabs) with passive Sorbothane feet (Thorlabs) placed on a durometer 70 Sorbothane sheet. This assembly was placed on a rack shelf within the PoP cage where the utilized dark fiber was terminated in a standard fiber-optic patch panel with SC-UPC connection. Connection to the Silixa iDAS was made using an SC-UPC/SC-APC single-mode patch cable. An optical time-domain reflectometer (OTDR) was used to evaluate fiber integrity prior to recording. An OTDR trace measured a total loss of 20.8 dB over the full fiber length of 101 km at 1550nm, or an average loss of 0.2059 dB/km.

0.2 Details of data collection, computing, and processing infrastructure

As mentioned in the main manuscript, the data was collected at 500 Hz in the iDAS native format in the form of raw 1 minute records at 2m spatial sampling. Files were written to a local USB3-connected 8 or 16 TB external hard drive. To maintain continuity of the dataset, hard drives were replaced on a weekly or biweekly basis and manually transferred from West Sacramento CA to Berkeley CA, where the data were uploaded to a local RAID storage server using the Globus protocol (https://www.globus.org/, last accessed: 2018-05-21) from a networked data transfer node. The storage server was linked to five RAID6 disk arrays and the full dataset was striped to improve performance. Primary processing was carried out on a 32-core GPU server connected to the storage server via a fast GB switch. Final results were visualized using a combination of MATLAB (Mathworks) and the ObsPy package.

0.3 Processing Framework & Parameters for Ambient Noise Analysis

As mentioned in the primary manuscript, we adopted the ambient noise surface wave processing and inversion approach detailed in[20] with the steps shown in Supplemental Fig. 9. Ambient noise interferometry was performed on sequential 120 m long subsections of the array to provide a combination of sufficient spectral resolution and a useful spatial resolution short enough for 1D analysis during inversion. In each subsection, the southernmost channel was treated as the virtual source and cross-correlated with the remainder of the channels.

To prepare the raw records for noise correlation, static offsets and linear trends were removed, followed by temporal decimation down to a coarser sampling rate of 8 ms. Next, a temporal normalization with running-absolute-mean was applied over a 0.5-second running window. The frequency content of the data between 0.5 Hz and 18 Hz was then balanced with a spectral whitening step. Finally, in each of the 1-minute records, the noise of the virtual-source channel was cross-correlated with the rest of the channels' records to form a common virtual-source gather. To achieve good SNR with a minimal stack count, phase-weighted stacking ($\nu = 0.5$) was used and a stack count of 40 was sufficient for reaching temporal stability.

A slant stack was then applied to the stacked common virtual-shot gathers to transform the data from space-time domain to frequency-velocity domain. Multimodal dispersion curves were extracted from spectra maxima as the input of the final inversion step. Multimodal inversion of surface waves was carried out using the Haskell-Thomson matrix determinant method. Because

of the nonlinear nature of the problem and the low computational costs of the determinant method, Monte Carlo sampling was used based on a model pool size of 1×10^6. A four-layer model configuration, in which we solved for V_s velocities and layer thicknesses. Search bounds of the model parameters are shown in Table 1. Each set of the inversions took 1.5 minutes on 24 cores (2.3 GHz Intel Xeon processors).

Table 1. Upper and lower bounds in Monte Carlo sampling of the inversion variables.

Layer	$V_{s_{min}}$ (m/s)	$V_{s_{max}}$ (m/s)	h_{min} (m)	h_{max} (m)
1	100	300	1	6
2	200	800	2	30
3	500	2000	2	30
4	1500	2500	–	–

0.4 Processing Framework & Parameters for Earthquake Analysis

We identified earthquake records in the continuous raw DAS dataset using catalogued origin times and approximate travel times to Sacramento for the 1-D iasp91 Earth velocity model. 1-minute duration earthquake records were merged together, and then, if desired, stacked with a mean average of traces over a specified length (100 m=50 traces averaged and plotted at the midpoint), prior to the application of a specified bandpass filter to remove unwanted or uninteresting signals. In Fig. 5a, the iasp91 model was again used to calculate the phase arrival angles with respect to vertical. Fig. 5b shows one stacking effect.

0.5 Data on Reference Wells

Data on the reference groundwater monitoring well discussed was acquired from the CASGEM database. As mentioned in the text, the well is referred to as the Sac Bypass Shallow Well (State well ID 09N04E20-N001M and CASGEM ID 25619). The well is located in Yolo County at 38.6062 N, -121.5602 W with a surface elevation of 6.55 m (21.49 ft) above sea level; the well is associated with the Yolo County Water Resources Association (WRA) with measurements conducted by the CA Department of Water Resources (DWR). The well is completed with slotted PVC and a sandpack over a 6.1 m (20 ft) interval from 24.4 to 30.5 m below ground surface.

References

1. Quesnel, H. & Curran, M. Shelterwood harvesting in root-disease infected stands—post-harvest soil disturbance and compaction. *For. Ecol. Manag.* **133**, 89–113 (2000).
2. Le Hégarat-Mascle, S., Zribi, M., Alem, F., Weisse, A. & Loumagne, C. Soil moisture estimation from ers/sar data: Toward an operational methodology. *IEEE Transactions on Geosci. Remote. Sens.* **40**, 2647–2658 (2002).
3. Chaussard, E. *et al.* Remote sensing of ground deformation for monitoring groundwater management practices: Application to the santa clara valley during the 2012–2015 california drought. *J. Geophys. Res. Solid Earth* **122**, 8566–8582 (2017).
4. Wahr, J., Swenson, S., Zlotnicki, V. & Velicogna, I. Time-variable gravity from grace: First results. *Geophys. Res. Lett.* **31** (2004).
5. Xiao, M. *et al.* How much groundwater did california's central valley lose during the 2012–2016 drought? *Geophys. Res. Lett.* **44**, 4872–4879 (2017).
6. Houborg, R., Rodell, M., Li, B., Reichle, R. & Zaitchik, B. F. Drought indicators based on model-assimilated gravity recovery and climate experiment (grace) terrestrial water storage observations. *Water Resour. Res.* **48** (2012).
7. Lecocq, T., Longuevergne, L., Pedersen, H. A., Brenguier, F. & Stammler, K. Monitoring ground water storage at mesoscale using seismic noise: 30 years of continuous observation and thermo-elastic and hydrological modeling. *Sci. Reports* **7**, 14241 (2017).
8. Long, J. *et al.* An independent scientific assessment of well stimulation in california volume ii: Potential environmental impacts of hydraulic fracturing and acid stimulations. Tech. Rep., California Council on Science and Technology (2015).
9. Reilly, J. *et al.* Mobile phones as seismologic sensors: Automating data extraction for the ishake system. *IEEE Transactions on Autom. Sci. Eng.* **10**, 242–251 (2013).
10. Kong, Q., Allen, R. M., Schreier, L. & Kwon, Y.-W. Myshake: A smartphone seismic network for earthquake early warning and beyond. *Sci. advances* **2**, e1501055 (2016).

11. Crooks, A., Croitoru, A., Stefanidis, A. & Radzikowski, J. # earthquake: Twitter as a distributed sensor system. *Transactions GIS* **17**, 124–147 (2013).

12. Cochran, E. S., Lawrence, J. F., Christensen, C. & Jakka, R. S. The quake-catcher network: Citizen science expanding seismic horizons. *Seismol. Res. Lett.* **80**, 26–30 (2009).

13. Jamali-Rad, H. & Campman, X. Iot-based wireless networking for geoscience applications. In *79th EAGE Conference and Exhibition 2017-Workshops* (2017).

14. Durairajan, R., Barford, P., Sommers, J. & Willinger, W. Intertubes: A study of the us long-haul fiber-optic infrastructure. In *ACM SIGCOMM Computer Communication Review*, vol. 45, 565–578 (ACM, 2015).

15. Nagel, J. A., Woodward, S. & Zou, L. Long-term monitoring of local temperature and strain changes in a buried fiber-optic cable using brillouin otdr. In *Frontiers in Optics*, FMC1 (Optical Society of America, 2010).

16. Daley, T., Miller, D., Dodds, K., Cook, P. & Freifeld, B. Field testing of modular borehole monitoring with simultaneous distributed acoustic sensing and geophone vertical seismic profiles at citronelle, alabama. *Geophys. Prospect.* **64**, 1318–1334 (2016).

17. Becker, M., Ciervo, C., Cole, M., Coleman, T. & Mondanos, M. Fracture hydromechanical response measured by fiber optic distributed acoustic sensing at millihertz frequencies. *Geophys. Res. Lett.* **44**, 7295–7302 (2017).

18. Daley, T. M. *et al.* Field testing of fiber-optic distributed acoustic sensing (das) for subsurface seismic monitoring. *The Lead. Edge* **32**, 699–706 (2013).

19. Mateeva, A. *et al.* Distributed acoustic sensing for reservoir monitoring with vertical seismic profiling. *Geophys. Prospect.* **62**, 679–692 (2014).

20. Dou, S. *et al.* Distributed acoustic sensing for seismic monitoring of the near surface: A traffic-noise interferometry case study. *Sci. reports* **7**, 11620 (2017).

21. Lancelle, C. *Distributed Acoustic Sensing for Imaging Near-Surface Geology and Monitoring Traffic at Garner Valley, California* (The University of Wisconsin-Madison, 2016).

22. Zeng, X. *et al.* Properties of noise cross-correlation functions obtained from a distributed acoustic sensing array at garner valley, california. *Bull. Seismol. Soc. Am.* **107**, 603–610 (2017).

23. Lindsey, N. J. *et al.* Fiber-optic network observations of earthquake wavefields. *Geophys. Res. Lett.* (2017).

24. Martin, E. R. *et al.* Seismic monitoring leveraging existing telecom infrastructure at the sdasa: Active, passive, and ambient-noise analysis. *The Lead. Edge* **36**, 1025–1031 (2017).

25. Schmandt, B. & Clayton, R. W. Analysis of teleseismic p waves with a 5200-station array in long beach, california: Evidence for an abrupt boundary to inner borderland rifting. *J. Geophys. Res. Solid Earth* **118**, 5320–5338 (2013).

26. Michaels, P. & Barrash, W. The anomalous behavior of sh-waves across the water table. In *9th EEGS Symposium on the Application of Geophysics to Engineering and Environmental Problems* (1996).

27. Wiemer, S. & Wyss, M. Minimum magnitude of completeness in earthquake catalogs: Examples from alaska, the western united states, and japan. *Bull. Seismol. Soc. Am.* **90**, 859–869 (2000).

28. Nanjo, K. *et al.* Analysis of the completeness magnitude and seismic network coverage of japan. *Bull. Seismol. Soc. Am.* **100**, 3261–3268 (2010).

29. Pasyanos, M. E., Dreger, D. S. & Romanowicz, B. Toward real-time estimation of regional moment tensors. *Bull. Seismol. Soc. Am.* **86**, 1255–1269 (1996).

30. Berkeley digitial seismic network, uc berkeley seismological laboratory. dataset (1991). DOI doi10.7932/BDSN.

31. Felzer, K. R. Calculating california seismicity rates. Tech. Rep., Geological Survey (US) (2008).

32. Hutton, K., Woessner, J. & Hauksson, E. Earthquake monitoring in southern california for seventy-seven years (1932–2008). *Bull. Seismol. Soc. Am.* **100**, 423–446 (2010).

33. Becker, M., Coleman, T., Ciervo, C., Cole, M. & Mondanos, M. Fluid pressure sensing with fiber-optic distributed acoustic sensing. *The Lead. Edge* **36**, 1018–1023 (2017).

34. Kuvshinov, B. Interaction of helically wound fibre-optic cables with plane seismic waves. *Geophys. Prospect.* **64**, 671–688 (2016).

35. Wu, X. *et al.* Compressional-and shear-wave studies of distributed acoustic sensing acquired vertical seismic profile data. *The Lead. Edge* **36**, 987–993 (2017).

36. Li, Z., Peng, Z., Hollis, D., Zhu, L. & McClellan, J. High-resolution seismic event detection using local similarity for large-n arrays. *Sci. reports* **8**, 1646 (2018).

37. Addair, T., Dodge, D. A., Walter, W. & Ruppert, S. D. Large-scale seismic signal analysis with hadoop. *Comput. & Geosci.* **66**, 145–154 (2014).

38. Chen, P. *et al.* psin: A scalable, parallel algorithm for seismic interferometry of large-n ambient-noise data. *Comput. & Geosci.* **93**, 88–95 (2016).

Acknowledgements

This work was supported by the Laboratory Directed Research and Development (LDRD) Program of Lawrence Berkeley National Laboratory under U.S. Department of Energy Contract No. DE-AC02-05CH11231. This research used resources of the ESnet Dark Fiber Testbed, which is supported by the Office of Science of the U.S. Department of Energy under contract DE-AC02-05CH11231. Nate Lindsey was supported by the National Science Foundation Graduate Research Fellowship under Grant No. DGE 1106400. We would like to thank Silixa for long-term support of our DAS acquisition efforts. We would like to thank Dr. Sebastiano Foti (Politecnino di Torino) for providing the original version of the multimodal surface-wave inversion code utilized in our ambient noise analysis as well as developing the inversion concept. Finally, we would like to thank CenturyLink for providing installation protocol details on the network section utilized in this study.

Author contributions statement

J. Ajo-Franklin developed the project concept, participated in deployment and processing, led development of the manuscript, and supervised all personnel. S. Dou led data pre-processing effort, led interferometric analysis, participated in deployment, and contributed to the manuscript. N. Lindsey led field deployment, led earthquake seismology analysis, and contributed to the manuscript. B. Freifeld participated in project development and contributed to the manuscript. T.M. Daley participated in project development and contributed to the manuscript. C. Ulrich and M. Robertson participated in deployment and reviewed the manuscript. C. Tracy and I. Monga supported network deployment and reviewed the manuscript. All authors have approved the manuscript in the submitted form.

Data availability statement

Due to the very large size of this dataset, only decimated raw components or processed subsections are available upon request.

Competing interests statement

None of the authors have competing financial interests.

Supplementary Material

0.6 Ambient Noise Analysis Processing Flow

Figure 9 below provides a schematic of the ambient noise processing steps described in the methods section.

0.7 Secondary Data Sources

Historical groundwater level data was obtained from public domain sources including the California Statewide Groundwater Elevation Monitoring (CASGEM) database [http://www.water.ca.gov/groundwater/casgem/]. Realtime groundwater data was obtained from the California Data Exchange Center (CDEC) [https://cdec.water.ca.gov/]. Completion report and driller's logs were obtained from the CA Department of Water Resources (DWR) Well Completion Report Map Application [https://gis.water.ca.gov/app/wcr/]. Topographic data and map layers used in Fig. 1 were obtained from the USGS National Map project [https://nationalmap.gov/].

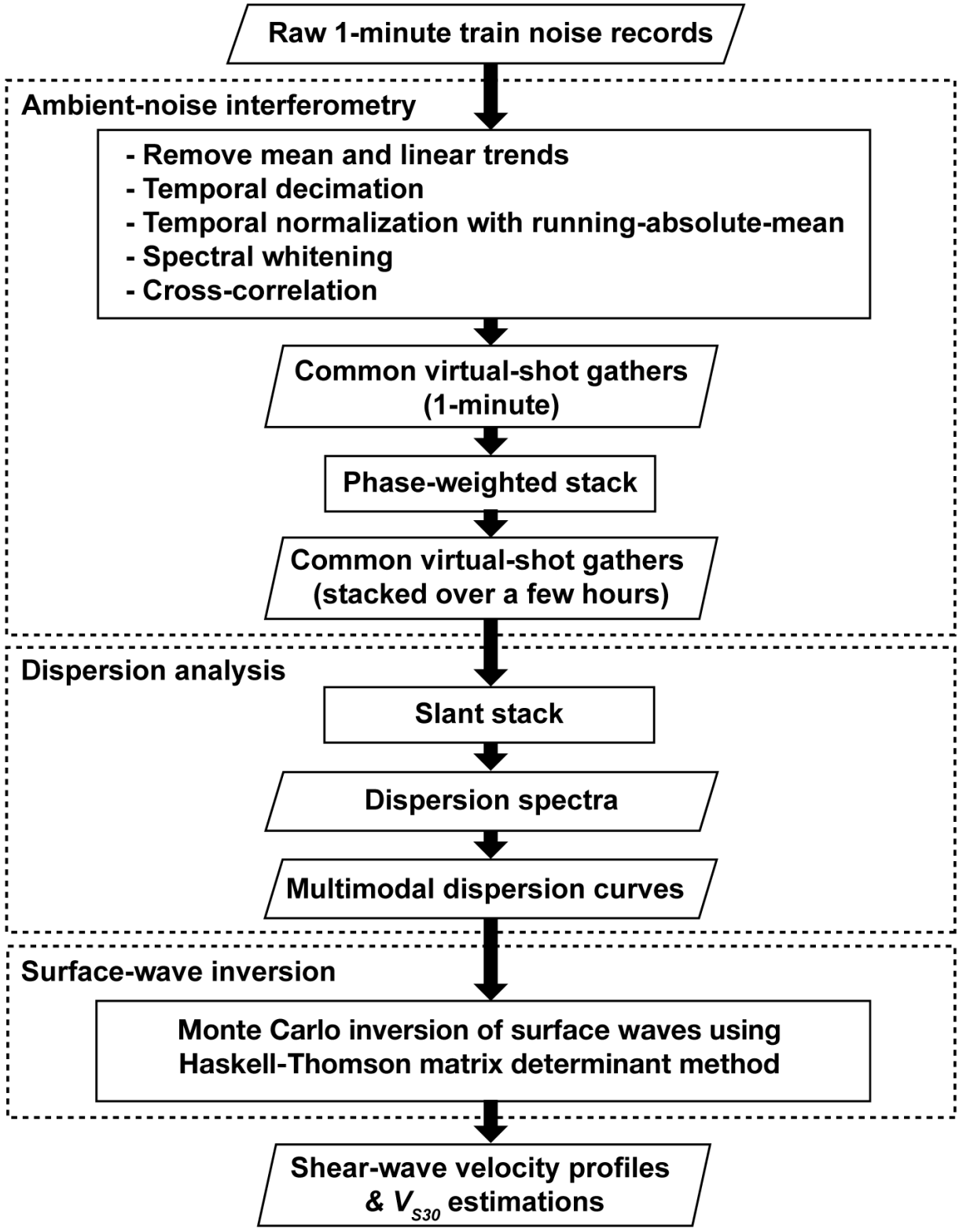

Figure 9. Ambient noise processing flow for near-surface V_s reconstructions.